Chemical Engineering Journal 466 (2023) 143347

Contents lists available at ScienceDirect

Chemical Engineering Journal

journal homepage: www.elsevier.com/locate/cej

Direct conversion of CH_4 and CO_2 to alcohols using plasma catalysis over $Cu/Al(OH)_3$ catalysts

Li Wang [a,*], Yuezhao Wang [a], Linhui Fan [a], Hongli Xu [a], Bowen Liu [c], Jiaren Zhang [b], Yimin Zhu [a], Xin Tu [c,*]

[a] College of Environmental Sciences and Engineering, Dalian Maritime University, Dalian 116026, Liaoning, China
[b] Petrochemical Research Institute, China National Petroleum Corporation, Beijing 102206, China
[c] Department of Electrical Engineering and Electronics, University of Liverpool, Liverpool L69 3GJ, UK

ARTICLE INFO

Keywords:
Plasma catalysis
Dry reforming of methane
CO_2 conversion
Biogas conversion
Alcohols
Cu-based catalysts

ABSTRACT

The direct conversion of CH_4 and CO_2 into high-value alcohols is a highly desirable route for efficiently utilizing these two C1 sources while mitigating greenhouse gas emissions. However, this reaction is considered one of the most challenging research topics since it suffers from the contradiction between thermodynamics and kinetics. In this study, plasma-catalytic conversion of CH_4 and CO_2 for the production of high-value alcohols, with methanol being the major liquid product, was achieved using Cu-based catalysts at ~190 °C and atmospheric pressure. Herein, the Cu-based catalysts were tuned by controlling the support material ($Al(OH)_3$, γ-Al_2O_3, TiO_2 and CeO_2), calcination temperature (400–600 °C) and copper loading (1–20 wt%) to promote alcohol production in this reaction. The results show that the 5 wt% $Cu/Al(OH)_3$ calcined at 540 °C exhibited the highest selectivity of alcohols (~38%), which is the best result achieved so far in the presence of a catalyst. Catalyst characterization results reveal that the redox capacity and valence state of the copper species play a crucial role in tuning the product distribution. The $Cu/Al(OH)_3$ catalyst with strong redox capacity and abundant Cu^{2+} species significantly improves the selectivity of alcohols. Interestingly, the predominant alcohol gradually shifts from methanol to ethanol with increasing copper loading, and the optimal copper loading for producing methanol and ethanol was found to be 5 wt% and 15 wt%, respectively. This work provides valuable insights for designing efficient catalysts to tune the production of alcohols through the single-step plasma-catalytic conversion of CH_4 and CO_2.

1. Introduction

Anthropogenic causes are widely recognized as the primary drivers of climate change, attributed to activities such as the combustion of fossil fuels, deforestation and unsustainable land practices. Various strategies have already been implemented to migrate climate change, including soil remediation, greenhouse gas recycling, and more. [1–5]. Methane (CH_4) and carbon dioxide (CO_2) are two of the major greenhouse gases, contributing to global warming and climate change. The utilization of CH_4 and CO_2 as carbon sources for the production of valuable chemicals and fuels has become increasingly important to achieve a sustainable low-carbon economy and carbon–neutral ecosystem. The plasma-driven dry reforming of CH_4 (DRM) has received increasing attention recently due to its advantages over conventional processes [6–10]. This promising process enables the direct and single step conversion of CH_4 and CO_2 into valuable oxygenates under mild conditions, eliminating the need for a two-step high-temperature and high-pressure process via syngas.

However, this emerging process for the synthesis of alcohols via DRM also faces great challenges. The resulting products are complex, containing CO, C_1-C_4 hydrocarbons and oxygenates (e.g., alcohols, acids, ketones, and aldehydes). Alcohols, which are valuable fuels and platform chemicals, represent a more efficient use of CH_4 and CO_2. Despite this promising potential, the current selectivity of alcohol production is still insufficient for industrial applications. Previous studies have investigated the conversion of CH_4 and CO_2 to oxygenates at low temperatures using a dielectric barrier discharge (DBD) plasma reactor [11]. The selectivity of oxygenates, including alcohols, acids, ketones and aldehydes, was found to vary depending on plasma parameters and reaction conditions, such as the discharge gap and CH_4/CO_2 feed ratio. Tosi and co-workers reported the formation of oxygenates in the plasma DRM reaction using a DBD reactor [12,13]. Methanol and ethanol were

* Corresponding authors.
E-mail addresses: liwang@dlmu.edu.cn (L. Wang), xin.tu@liv.ac.uk (X. Tu).

https://doi.org/10.1016/j.cej.2023.143347
Received 23 February 2023; Received in revised form 15 April 2023; Accepted 2 May 2023
Available online 5 May 2023

detected, but the selectivity of each oxygenate was not given. They evaluated the effect of discharge duty cycle and electrode type on the generation of acids (butanoic, propanoic, acetic and formic acid). Furthermore, the possible mechanisms for acid generation were investigated using density functional theory (DFT) calculations. Kolb et al. revealed that the addition of O_2 to the reaction mixture improved methanol formation in the DBD plasma DRM reaction using He as a diluent gas, with methanol selectivity reaching 1% at an O_2 content of 29% [14]. Krawczyk et al. reported that only methanol and ethanol were produced in a CH_4/CO_2 DBD plasma with and without packing materials (i.e., Al_2O_3, Fe/Al_2O_3, NaY and NaZSM-5), with the highest selectivity of alcohols being less than 3.5 % in the absence of packing materials [15]. Rahmani et al. found that increasing the Ar content in the feed gas decreased methanol selectivity, while the selectivity of isopropanol and ethanol initially increased and then decreased. However, the total yield of oxygenates was only 2–4 % of the total mass of the products in CH_4/CO_2 plasma [16]. Michielsen et al. investigated the influence of packing materials (ZrO_2, SiO_2, α-Al_2O_3 $BaTiO_3$, γ-Al_2O_3) on product distribution, and achieved 3% ethanol selectivity with γ-Al_2O_3 packing, but no methanol was detected [17]. Similarly, Gelves et al. evaluated the influence of different packing materials on alcohol selectivity, including Colombian natural zeolite, glass wool and a material composed of magnesium oxide and alumina. The highest selectivity of alcohols (7%), including methanol, ethanol, propanol and butanol, was achieved when the plasma was coupled with Colombian natural zeolite, with methanol being the major liquid product in this case [18].

Very recently, Fulcheri et al. reported that packing Fe/SiO_2 or Co/SiO_2 catalysts into CO_2/CH_4 plasma greatly promoted the formation of oxygenates with selectivity up to 40%, and the selectivity of alcohols reached 35% with 31% methanol in the presence of Fe/SiO_2 [19]. Shao and co-workers found that packing a NiAl-LDH/NF catalyst into CO_2/CH_4 plasma achieved 18% alcohol selectivity with 12% methanol [20]. They also discovered that oxygen vacancies can promote the formation of methanol, whereas metallic Co species are favorable for the production of acetic acid. The selectivity of alcohols reached ~15% when the P-CoMgAl/NF catalyst was packed [21]. Wang et al. investigated the acidic properties of the catalysts on the total selectivity of oxygenates and carbon deposition in the plasma-catalytic DRM reaction [22]. They found that a Pt/UZSM5 catalyst with 100% weak acidic sites exhibited a total oxygenate selectivity of up to 60%, including formaldehyde, methanol, ethanol, and acetone, but the specific distribution of these oxygenates was not given. Chen and colleagues conducted a similar study, but with CO_2 and C_2H_6 as the feed gases, and discovered that alcohols, aldehydes, and acids were obtained with a maximum total oxygenate selectivity of 12%, which matched well with the results obtained from chemical kinetic modeling [23]. Based on DFT calculations, Shirazi et al. reported the pathway of methanol formation on a crystalline Ni (1 1 1) surface in the plasma DRM reaction [24]. Mei et al. evaluated the activity of γ-Al_2O_3 supported catalyst in the plasma DRM reaction, and the highest total selectivity of liquid products was achieved at 14% with 9% alcohols over the Ni/γ-Al_2O_3 catalyst [25]. Liu et al. found the presence of a small amount of methanol, acetic acid and ethanol in the products during the plasma DRM reaction over Ni/BN catalysts [26]. Our previous work achieved an oxygenate selectivity of 50–60% with acetic acid as the major liquid product through developing a novel DBD reactor with a special water ground electrode [27]. Meanwhile, a selectivity of ~23% was obtained for alcohols, with methanol and ethanol being presented in nearly equal amounts. Our recent study revealed a synergy of Cu^+ species and Brønsted acid sites in acetic acid generation through the plasma-catalytic DRM reaction, whereas Cu^{2+} species favor alcohol production. The highest selectivity of alcohols (methanol, ethanol, propanol and butanol) reached 20%, with methanol being the major oxygenate [28].

In brief, increasing efforts are being made to investigate the one-step conversion of CH_4 and CO_2 into high-value alcohols, as it is a very promising and desirable process. While alcohols can be produced as the main liquid products in the plasma DRM reaction, achieving high selectivity for specific target alcohols remains challenging. Designing robust catalysts is generally considered as a key strategy for manipulating the distribution of products. However, there is currently a lack of understanding regarding the design of more efficient catalysts to control the selectivity of alcohol production. To date, the available information on catalyst design for this process is limited, and only a few catalysts have shown a favorable effect on alcohol formation.

Since copper is well recognized as the most active and selective component in catalysts for methanol synthesis from syngas, herein, a series of Cu-based catalysts were investigated to enhance the formation of alcohols during the plasma-catalytic DRM reaction at ~190 °C and atmospheric pressure. Different support materials ($Al(OH)_3$, γ-Al_2O_3, TiO_2 and CeO_2), calcination temperatures (400, 450, 500, 540 and 600 °C) and Cu loadings (1, 3, 5, 10, 15 and 20 wt%) were evaluated to optimize the catalysts for selective alcohol production. The catalysts were thoroughly characterized to gain insights into their properties and understand their influence on the plasma-catalytic production of alcohols via DRM. Finally, the key properties of the copper-based catalysts that determine alcohol production were discussed in detail.

2. Experimental

2.1. Catalyst preparation

The commercial $Al(OH)_3$ (205 m^2/g, ~10 nm), γ-Al_2O_3 (210 m^2/g, 5–10 nm), TiO_2 (300 m^2/g, ~5 nm) and CeO_2 (65 m^2/g, ~20 nm) were purchased from Shanghai Buwei Material Co., Ltd., China. All of the catalysts were prepared through the incipient wetness impregnation method. Specifically, taking 5 wt% Cu/TiO_2 for example, the TiO_2 support was firstly calcined at 400 °C for 3 h to remove any impurities (e.g., adsorbed H_2O). Then, the precursor $Cu(NO_3)_2{\cdot}3H_2O$ was dissolved in deionized water, and the TiO_2 powder was added under stirring for 5 h aging at room temperature. The mixture was then filtered, and the obtained paste was dried at 120 °C overnight. Finally, the sample was calcined at 540 °C for 5 h in air, and the catalyst is denoted as Cu/TiO_2. The preparation procedure for Cu/γ-Al_2O_3 and Cu/CeO_2 catalysts followed the same method as for Cu/TiO_2. However, the $Cu/Al(OH)_3$ catalyst was prepared with a slightly different procedure. The only difference in the preparation of the $Cu/Al(OH)_3$ catalyst was the use of a lower calcination temperature of 250 °C to preserve the phase state of $Al(OH)_3$ and eliminate impurities such as adsorbed H_2O from the commercial $Al(OH)_3$.

The preparation of the 5 wt% $Cu/Al(OH)_3$ catalysts with different calcination temperatures followed a similar procedure to that of the above-mentioned $Cu/Al(OH)_3$ catalyst, with the exception of the final step. The resulting sample was calcined at 400, 450, 500, 540 and 600 °C for 5 h in air, respectively.

The preparation of the $Cu/Al(OH)_3$ catalysts with different Cu loadings (1, 3, 5, 10, 15 and 20 wt%) followed a similar procedure to that of the 5 wt% $Cu/Al(OH)_3$ catalyst calcined at 540 °C. The main difference lied in the amount of $Cu(NO_3)_2{\cdot}3H_2O$ used to create the precursor solution. This resulted in different Cu loadings of 1, 3, 5, 10, 15 and 20 wt%. The resulting sample was then calcined at 540 °C for 5 h in air to obtain the final catalysts.

2.2. Catalytic test

The conversion of CH_4 and CO_2 was carried out at atmospheric pressure using a DBD reactor, which was similar to the experimental setup described in our previous studies [27,29]. However, the DBD reactor used in this study consisted of a coaxial quartz cylinder and bare-metal electrodes. A quartz tube (10 mm o.d. × 8 mm i.d.) severed as the reactor shell and dielectric barrier, while the outer ground electrode was a 0.1 mm thick Al foil tightly wrapped around the outer surface of the quartz tube. The inner high-voltage electrode was a stainless-steel rod

with an outer diameter of 2 mm, positioned along the axis of the quartz tube. The discharge length was 45 mm with a discharge gap of 3 mm, and the catalyst was placed directly within the discharge area. The flow rate of CH_4 and CO_2 was regulated using mass flow controllers with a CH_4/CO_2 mole ratio of 1:1 and a total flow rate of 40 mL/min. The feed gas first passed through a water bath with a saturated vapor pressure of 47.3 kPa before flowing into the DBD plasma reactor. The discharge frequency was fixed at 9 kHz, and the reaction proceeded for 2 h. A cold trap, consisted of anhydrous ethanol and liquid nitrogen, was placed at the exit of the DBD reactor to condense the liquid products. The gaseous products and liquid products were analyzed quantitatively, online and offline respectively, using a gas chromatograph (Shimadzu GC-2014C) equipped with a flame ionized detector (FID) and a thermal conductivity detector (TCD). The FID was connected to a free fatty acid polyester (FFAP) capillary column (30 m × 0.32 mm × 0.5 um in length, inner diameter and thickness) and an Al_2O_3 column (2 m × 4 mm in length and inner diameter), which were used to analyze liquid products offline and C_1-C_4 hydrocarbons online, respectively. The TCD was connected to a TDX-01 column (2 m × 4 mm in length × inner diameter), which was used to analyze CO, CO_2 and CH_4 online. Gas volume changes before and after the reaction were measured using a flow meter.

In this work, the conversion of CH_4 and CO_2, and the selectivity of the main gaseous products (CO, C_2-C_4 hydrocarbons) and oxygenate (CH_3COOH, CH_3COCH_3, CH_3CHO and C_1-C_4 alcohols) were used as evaluation indicators. The specific calculation equations used for these indicators are shown below.

$$X_{CO_2}(\%) = \frac{\text{moles of } CO_2 \text{ converted}}{\text{moles of initial } CO_2} \times 100\% \quad (1)$$

$$X_{CH_4}(\%) = \frac{\text{moles of } CH_4 \text{ converted}}{\text{moles of initial } CH_4} \times 100\% \quad (2)$$

$$S_{CO}(\%) = \frac{\text{moles of CO produced}}{\text{moles of } CH_4 \text{ converted} + \text{moles of } CO_2 \text{converted}} \times 100\% \quad (3)$$

$$S_{C_xH_y}(\%) = \frac{x \times \text{moles of } C_xH_y \text{ produced}}{\text{moles of } CH_4 \text{ converted} + \text{moles of } CO_2 \text{converted}} \times 100\% \quad (4)$$

$$S_{Oxygenates}(\%) = 100\% - \left(S_{CO} + S_{C_xH_y}\right) \quad (5)$$

$$S_{CH_3COOH}(\%) = \frac{2 \times \text{moles of } CH_3COOH \text{ produced}}{\text{moles of total oxygenates produced}} \times S_{Oxygenates} \quad (6)$$

$$S_{CH_3COCH_3}(\%) = \frac{3 \times \text{moles of } CH_3COCH_3 \text{ produced}}{\text{moles of total oxygenates produced}} \times S_{Oxygenates} \quad (7)$$

$$S_{CH_3CHO}(\%) = \frac{2 \times \text{moles of } CH_3CHO \text{ produced}}{\text{moles of total oxygenates produced}} \times S_{Oxygenates} \quad (8)$$

$$S_{C_{1-4}OH}(\%) = \frac{\text{carbon number} \times \text{moles of alcohols produced}}{\text{moles of total oxygenates produced}} \times S_{Oxygenates} \quad (9)$$

2.3. Catalyst characterization

The physicochemical properties of the Cu-based catalysts were analyzed using various characterization techniques. The crystalline structure of the catalysts was determined by X-ray powder diffraction (XRD) using an X-ray diffractometer (Rigaku D-Max 2400) with Cu K_α radiation ($\lambda = 0.15406$ nm). The scan range was set from 5 to 80° (2θ) with a step size of 0.02° and a scanning speed of 10° min^{-1}. High resolution transmission electron microscopy (HRTEM) images of the catalyst were recorded using JEOL-JSM-2100F (Tecnai G2 F30 S-Twin) with an energy dispersive X-ray spectrometer (EDXS) at 200 kV acceleration voltage. The composition of the catalysts was measured by X-ray fluorescence spectroscopy (XRF) on a S8 TICER X (BRUKER AXS, DE) instrument. The valence state of the copper species in the catalysts was investigated by X-ray photoelectron spectroscopy (XPS) using a Thermo ESCALAB Xl + spectrometer. The redox properties of the catalysts were determined through H_2 temperature-programmed reduction (H_2-TPR) using a chemisorption instrument (Quantachrome ChemBET 3000). The TPR analysis was carried out in a H_2/Ar mixture flow (10 vol% H_2, 120 mL/min) from room temperature to 800 °C at a heating rate of 10 °C/min. The H_2 consumption, as a function of temperature, was monitored by a TCD through monitoring the H_2 concentration in the tail gas.

3. Results and discussion

3.1. Dependence of alcohol generation on support of Cu-based catalysts.

Fig. 1 shows the effect of support material on alcohol selectivity in the plasma-catalytic DRM reaction. The product contains CO, hydrocarbons and oxygenates regardless of the catalyst used (Fig. 1(a)). However, the supports have a significant impact on the distribution of products. The selectivity of oxygenate increases in the sequence of Cu/CeO_2 < Cu/TiO_2 < Cu/γ-Al_2O_3 < $Cu/Al(OH)_3$, while CO shows the opposite trend. Among these Cu-based catalysts, $Cu/Al(OH)_3$ displays the highest selectivity of oxygenate (~44%), which contains alcohols, acetic acid, acetone and acetaldehyde, with alcohols being the major liquid product, as presented in Fig. 1(b). Notably, alcohols, including methanol, ethanol, propanol and butanol, account for ~38% of the total product selectivity . This is the highest value reported so far in the presence of a catalyst.

Fig. 1(c) shows the distribution of gaseous hydrocarbon products, with ethane being the most abundant, followed by propane. This finding suggests the presence of a C-C coupling reaction over these Cu-based catalysts, particularly with the Cu/CeO_2 catalyst showing a more pronounced effect. The formation of ethane and propane mainly originates from the C-C coupling of CH_4, as supported by the literature [30] and conversion results, since Cu/CeO_2 shows the lowest conversion of CO_2 but a high CH_4 conversion, as shown in Fig. 1(d). Conversely, $Cu/Al(OH)_3$ exhibits the highest conversions of both CH_4 and CO_2, as well as the highest selectivity of alcohols in Fig. 1(b). Therefore, the coupling of the $Cu/Al(OH)_3$ catalyst with plasma enables the most effective conversion of CH_4 and CO_2 into alcohols.

To reveal the relationship between the support material and product distribution in the plasma-catalytic DRM reaction over Cu-based catalysts, the physicochemical properties of these catalysts were characterized using a variety of techniques, including XRF, XRD, HRTEM, H_2-TPR, and XPS. As presented in Table 1, the Cu content of the $Al(OH)_3$-, γ-Al_2O_3- and TiO_2-supported catalysts is similar (~6 wt%), while the CeO_2-supported catalysts shows a lower Cu content (~5 wt%). The HRTEM images in Fig. 2 show that Cu mainly presents as crystal CuO on the CeO_2, TiO_2, γ-Al_2O_3 and $Al(OH)_3$ supports. The lattice fringes of CuO were identified on these supports, with d-spacings of 0.27 nm and 0.23 nm via interference fringes, representing the CuO (1 1 0) and CuO (1 1 1) planes, respectively. However, the average copper particle size is difficult to be determined based on these HRTEM images.

The XRD pattern of Cu/γ-Al_2O_3 in Fig. 3(a) shows distinct diffraction peaks at 35.5° and 38.8° (JCPDS N° 45–0937), corresponding to the (11–1) and (1 1 1) planes of CuO [31], respectively. This is consistent with the results obtained from HRTEM analysis. However, the characteristic peaks of crystal CuO on the CeO_2, $Al(OH)_3$ and TiO_2 supports are very weak, indicating that the copper species are highly dispersed on these supports compared to γ-Al_2O_3.

Furthermore, H_2-TPR was performed to evaluate the redox properties of the Cu-based catalysts, which is one of the important factors in determining their catalytic activity. Generally, a lower reduction temperature indicates a strong redox capacity, which makes catalysts more active. By contrast, a higher reduction temperature signifies a weaker redox capacity and a more stable catalyst [32–36]. As shown in Fig. 3(b), the Cu-based catalysts exhibited hydrogen consumption peaks at different reduction temperatures depending on the supports, indicating

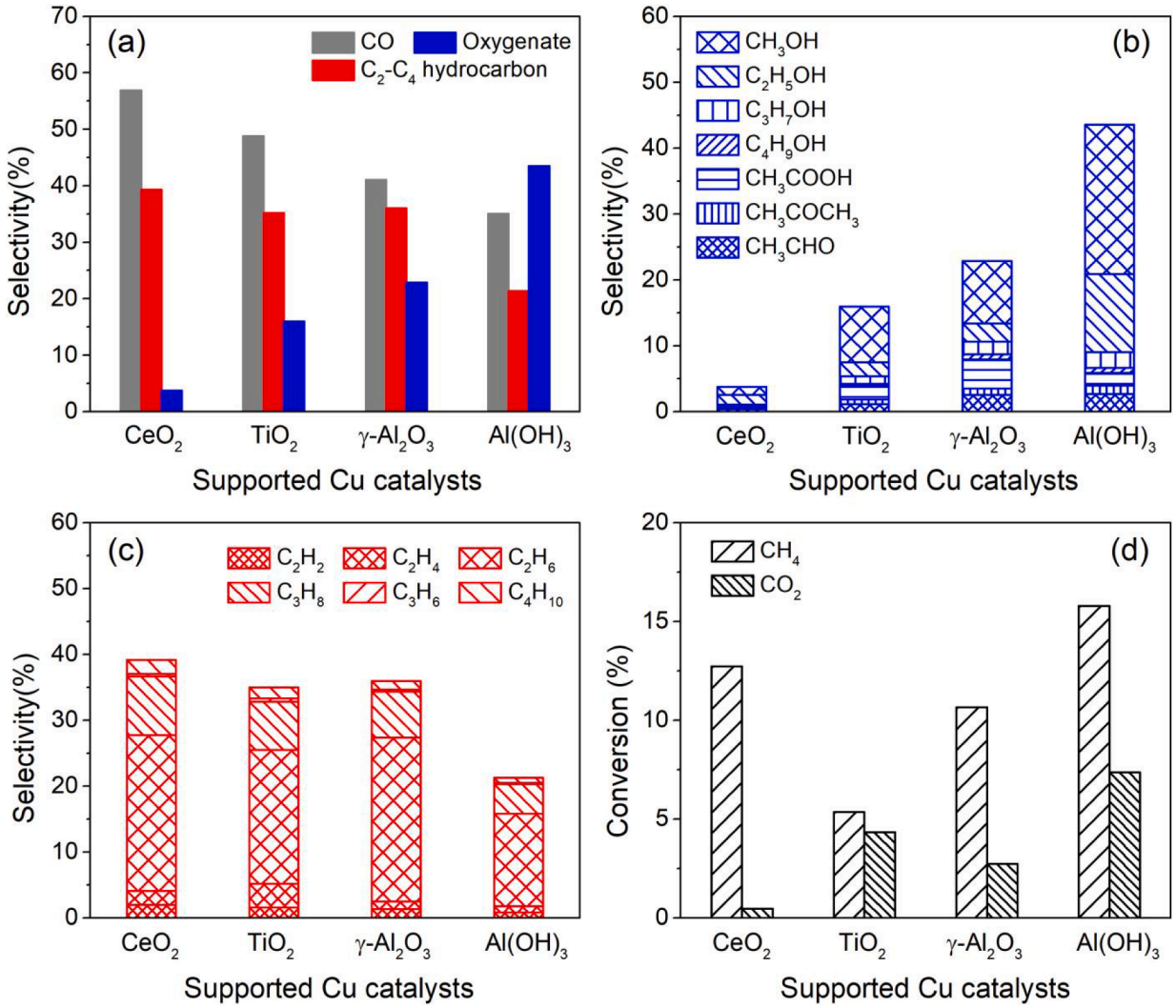

Fig. 1. Dependence of alcohol generation on support of Cu-based catalysts in plasma-catalytic DRM reaction. (a) Product distribution, (b) Selectivity of oxygenate, (c) Selectivity of gas products and (d) Conversion of CH_4 and CO_2 (reaction temperature was controlled at ~190 °C by tuning discharge power at ~5 W).

Table 1
Cu content of the supported Cu-based catalysts determined by XRF.

Catalyst	Cu/CeO_2	Cu/TiO_2	$Cu/\gamma\text{-}Al_2O_3$	$Cu/Al(OH)_3$
Cu content (%)	5.276	6.673	6.107	6.582

the presence of oxidized copper species with distinct reducible behaviors. Overall, the temperature of reduction peaks shifted gradually upward in the order of $Cu/Al(OH)_3 < Cu/\gamma\text{-}Al_2O_3 < Cu/TiO_2 < Cu/CeO_2$. According to previous studies [36], the reducible behavior of supported catalysts depends mainly on metal particle size and metal-support interaction. XRD results in Fig. 3(a) confirm that copper species were highly dispersed on the CeO_2, TiO_2 and $Al(OH)_3$. Therefore, the variations in reducible behavior of these Cu-based catalysts can be mainly attributed to their different interactions with the supports.

Additionally, the H_2-TPR profiles of these Cu-based catalysts show low-temperature and high-temperature reduction peaks (denoted as α and β, respectively) that correspond to two different types of copper species present in the catalysts. Among these catalysts, $Cu/Al(OH)_3$ shows the lowest reduction temperature for the α peak (less than150 °C), which is ascribed to the highly dispersed copper species that strongly interact with the support. On the other hand, the β peak (223 °C) is generally associated with the reduction of agglomerates of dispersed copper species, which have a relatively weak interaction with the support [37–40]. However, a much higher temperature of 300–400 °C is required for the reduction of bulk-phase CuO [36–38]. In contrast, Cu/CeO_2 shows the highest reduction temperature for both the α and β peaks, indicating the weakest interaction between copper and CeO_2. By correlating the reaction performances with the H_2-TPR results, it can be concluded that the $Cu/Al(OH)_3$ catalyst, with a strong redox capacity resulting from the easier reduction of highly dispersed copper species at low temperature, is favorable for alcohol generation. Conversely, the Cu/CeO_2 catalyst, with a weak redox capacity, shows poor activity for alcohol formation. Hence, the redox capacity of copper species is of great importance in determining the production of alcohols.

It is widely accepted that metal-support interaction can induce interfacial charge redistribution (i.e., electronic interaction) and/or interfacial atom transport (i.e., chemical interaction) [41–44]. Therefore, XPS analysis was used to determine the valence state of copper supported on $Al(OH)_3$, $\gamma\text{-}Al_2O_3$, TiO_2 and CeO_2, as shown in Fig. 4. The Cu $2p_{3/2}$ XPS fitting curves in Fig. 4(a) reveal the coexistence of Cu^{2+} and Cu^{+} in these Cu-based catalysts [45–47], with their relative contents varying depending on the support materials. In comparison to $Cu/Al(OH)_3$, the binding energy of the Cu $2p_{3/2}$ shifts towards a lower binding energy, particularly for the Cu/TiO_2 and Cu/CeO_2 catalysts (Fig. 4(b)). The shift in binding energy for supported catalysts is closely related to the degree of metal dispersion and the nature of the support materials

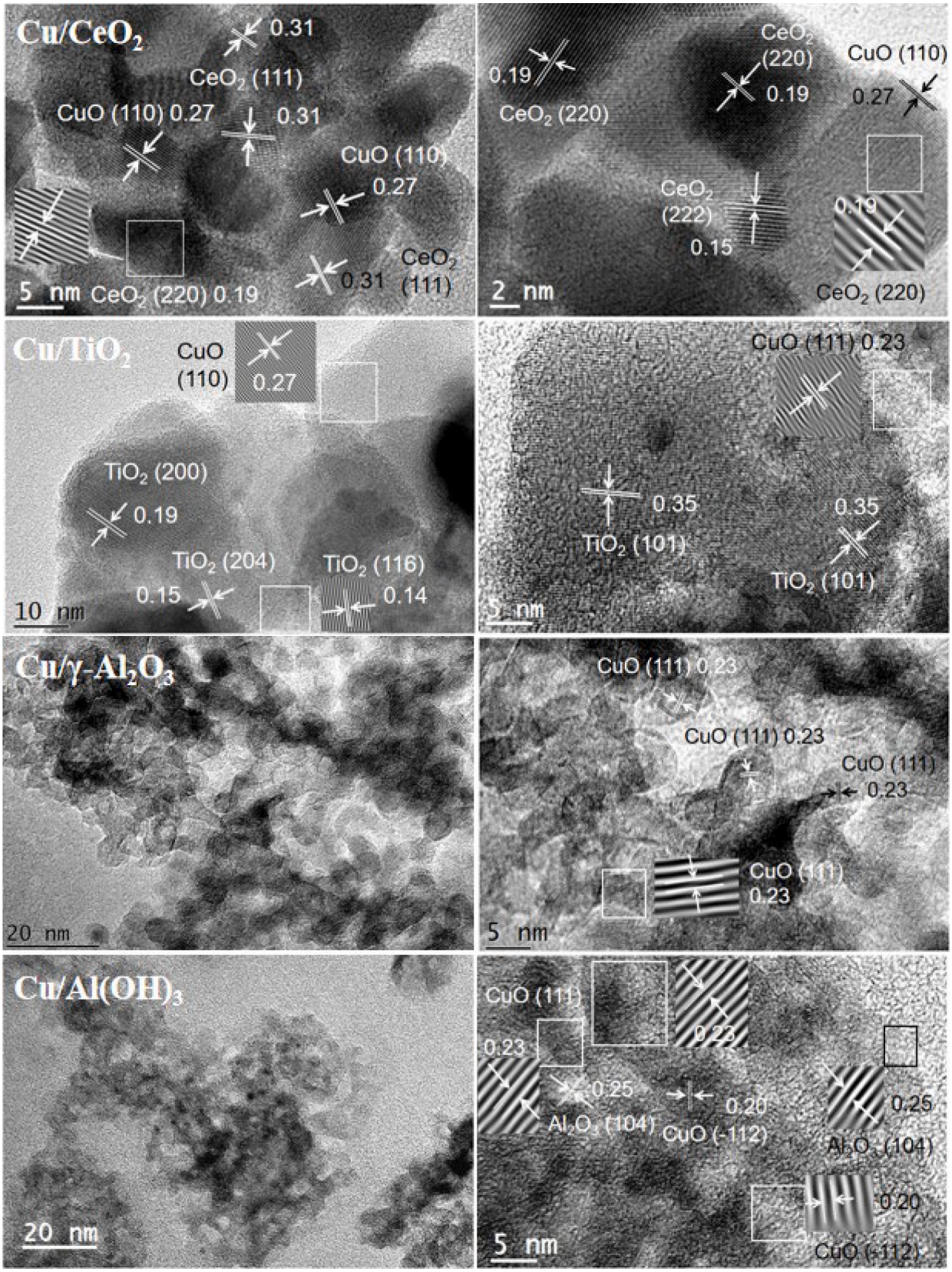

Fig. 2. HRTEM images of the supported Cu-based catalysts.

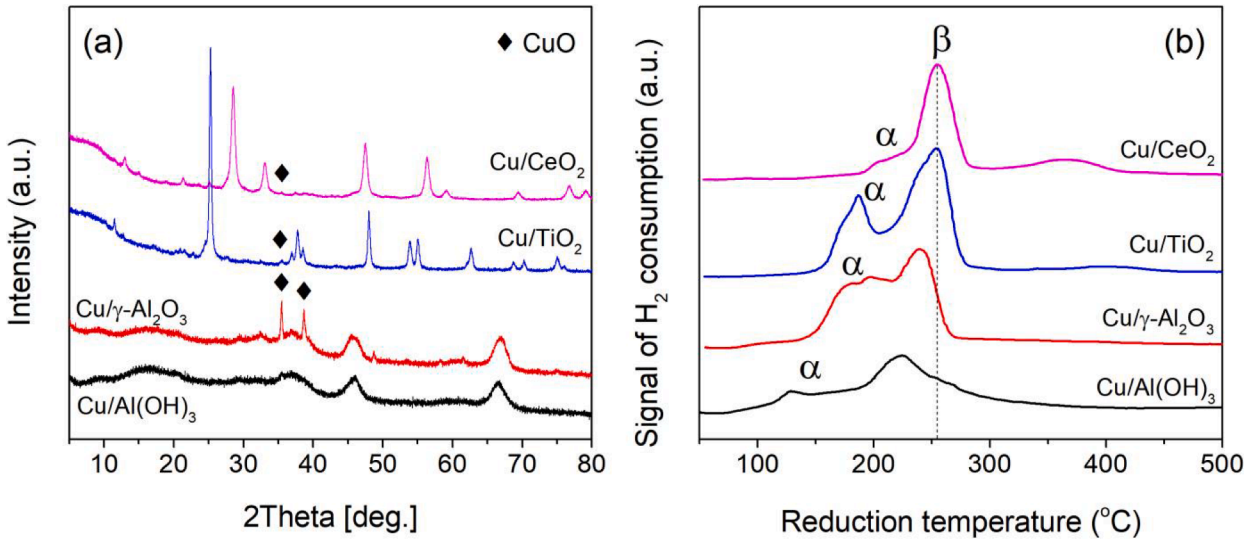

Fig. 3. (a) XRD patterns and (b) H_2-TPR profiles of the supported Cu-based catalysts.

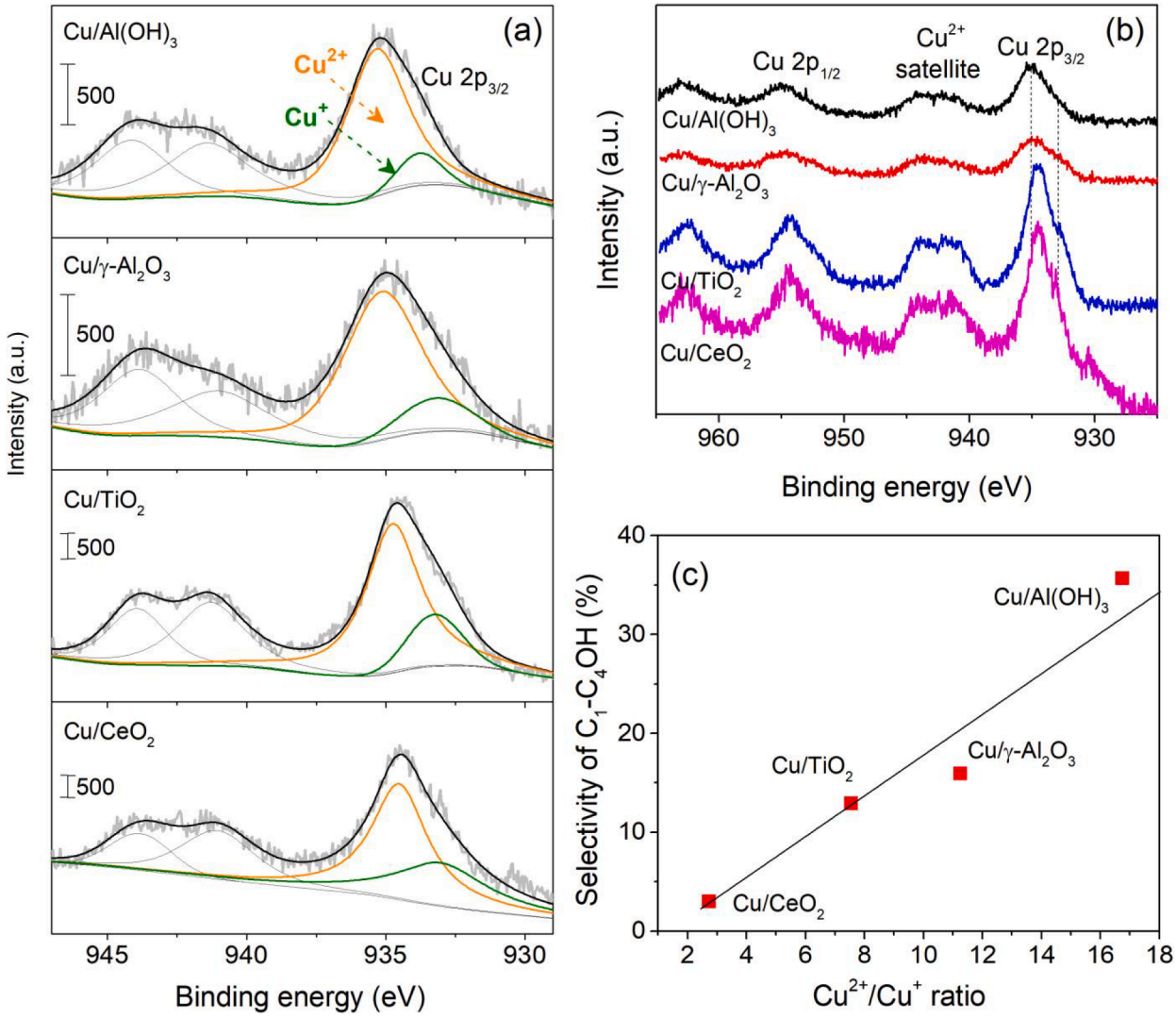

Fig. 4. XPS spectra of the supported Cu-based catalysts. (a) Deconvoluted Cu $2p_{3/2}$ XPS spectra, (b) Cu 2p XPS spectra and (c) Selectivity of alcohols as a function of Cu^{2+}/Cu^{+} ratio obtained in Fig. 4(a).

[45]. Considering the high dispersion of copper on these supports, except for γ-Al_2O_3, as demonstrated in Fig. 3(a), this shift observed in this study can be attributed to the influence of the support materials that have electronic interaction with copper. This is further supported by the presence of Cu^+ species in the Cu/TiO_2 and Cu/CeO_2 catalysts, as shown in Fig. 4(b). Compared to Al atom, Ce has a low electronegativity, which allows electrons to transfer from Ce to Cu (Ce-O-Cu) at the interface of copper and CeO_2, resulting in an increase in Cu^+ species [48]. These findings suggest that the support materials induce interfacial charge redistribution, i.e., electron transfer between copper and the support.

Generally, the electronic interaction between the metal and support significantly influences the catalytic activity of supported catalysts. Therefore, the selectivity of alcohols and the valence state of copper, expressed by the Cu^{2+} to Cu^+ ratio, are correlated in Fig. 4(c). It is worth noting that the selectivity of alcohols increases with an increasing Cu^{2+}/Cu^+ ratio, exhibiting an approximately linear relationship. Among the Cu-based catalysts, Cu/$Al(OH)_3$ with the highest Cu^{2+}/Cu^+ ratio exhibits the highest selectivity for alcohols. This is likely due to the strong redox capacity and abundant Cu^{2+} species present in this catalyst. In contrast, Cu/CeO_2 with the lowest Cu^{2+}/Cu^+ ratio, shows the lowest alcohol selectivity and CO_2 conversion, which may be due to the abundance of Cu^+ species on the surface of Cu/CeO_2, as suggested by Shen and coworkers [48]. They found that Cu^+ species on CeO_2 can bond with oxygen vacancies (O_v) of CeO_2 to form Cu^+-O_v-Ce^{3+} sites. These Cu^+ sites can chemically adsorb CO, while the O_v-Ce^{3+} sites can dissociatively activate H_2O, which enhances the water gas shift (WGS) reaction. This could explain the low conversion of CO_2 and selectivity of alcohols observed over Cu/CeO_2 (Fig. 1), since the produced CO can react with H_2O in the feed gas to form CO_2 over Cu/CeO_2 via the WGS reaction ($CO + H_2O \rightarrow CO_2 + H_2$), thus inhibiting the conversion of CO_2 and the formation of alcohols. In summary, the redox capacity and valence state of copper species in Cu-based catalysts play crucial roles in tuning alcohol selectivity in the plasma-catalytic DRM reaction. The Cu/$Al(OH)_3$ catalyst, in particular, is effective for alcohol generation due to its strong redox capacity and abundant Cu^{2+} species.

3.2. *Dependence of alcohol generation on calcination temperature of Cu/$Al(OH)_3$ catalyst.*

In this work, Cu/$Al(OH)_3$ has demonstrated the highest selectivity for alcohols among the Cu-based catalysts. Therefore, the catalytic performance of Cu/$Al(OH)_3$ was further investigated by varying the calcination temperatures. The phase state of $Al(OH)_3$ is strongly influenced by the calcination temperature, which in turn affects the catalytic activity of Cu/$Al(OH)_3$. Fig. 5 illustrates the influence of calcination temperatures (i.e., 400, 450, 500, 540 and 600 °C) on the performance

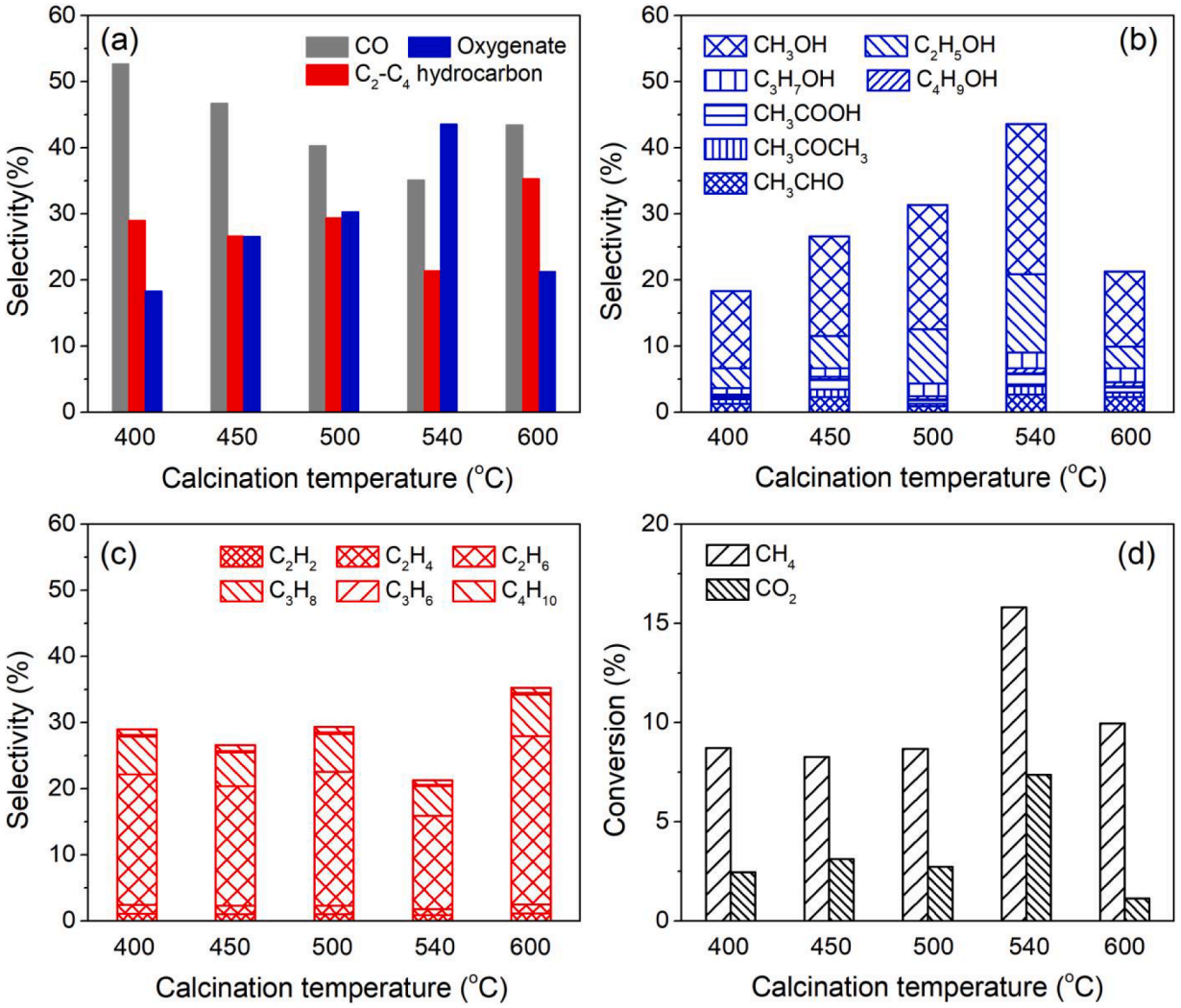

Fig. 5. Dependence of alcohol generation on calcination temperature of Cu/$Al(OH)_3$ catalyst in plasma-catalytic DRM reaction. (a) Product distribution, (b) Selectivity of oxygenate, (c) Selectivity of gas products and (d) Conversion of CH_4 and CO_2 (reaction temperature was controlled at ~190 °C by tuning discharge power at ~5 W).

of $Cu/Al(OH)_3$. Clearly, the selectivity of oxygenates initially increases and then decreases with increasing calcination temperature, while the opposite trend is observed for CO selectivity. The $Cu/Al(OH)_3$ catalyst calcined at 540 °C exhibited the highest selectivity for oxygenates but the lowest selectivity for CO. Although the calcination temperature significantly affects product selectivity, it has almost no effect on the distribution of oxygenates and hydrocarbons, as presented in Fig. 5(b) and (c). This means that alcohols and ethane consistently remain the major oxygenate and hydrocarbon, respectively, regardless of the calcination temperature. Furthermore, the highest conversions of CH_4 and CO_2 were achieved using the $Cu/Al(OH)_3$ catalyst calcined at 540 °C, as depicted in Fig. 5(d). These findings suggest that the calcination temperature can significantly affect the selectivity of the products but has minimal impact on their distribution in this study.

Fig. 6(a) shows the XRD patterns of the $Cu/Al(OH)_3$ catalysts calcined at different temperatures. The sample calcined at 400 °C exhibits an amorphous γ-AlOOH phase, as evidenced by a series of broad XRD diffraction peaks and relatively low diffraction intensities [49,50]. Even at a low calcination temperature of 400 °C, a diffraction peak of crystal CuO at 35.5° is observed [31], while another main diffraction peak at 38.8° for CuO overlaps with that of γ-AlOOH. Moreover, the characteristic peaks of CuO remain unchanged as the calcination temperature increases from 450 to 600 °C. However, when the calcination temperature exceeds 400 °C, the phase state of γ-AlOOH transforms into γ-Al_2O_3 due to further dehydroxylation [51]. Apart from the phase state change, the calcination temperature also significantly affects the redox capacity of the $Cu/Al(OH)_3$ catalysts, as evidenced by the H_2-TPR profiles in Fig. 6(b). The reduction temperature of the $Cu/Al(OH)_3$ catalyst initially decreased and then increased with increasing calcination temperature, with the turning point occuring at 540 °C. The $Cu/Al(OH)_3$ catalyst calcined at 540 °C showed the lowest reduction temperature, indicating the strongest interaction between copper and the $Al(OH)_3$ support, i.e., the strongest redox capacity. This strong interaction is mainly attributed to the dehydration of adjacent hydroxyl in $Al(OH)_3$, caused by the high calcination temperature, to form O layer termination, which induces the surface to be energetically unstable and enhances the strong interaction of copper with the O termination to form Cu-O-Al [42]. Conversely, the $Cu/Al(OH)_3$ catalyst calcined at 400 °C exhibited the weakest interaction between Cu and $Al(OH)_3$. In this case, the OH groups in $Al(OH)_3$ were partially retained at the calcination temperature of 400 °C (as demonstrated by XRD), which lowered the surface energy of the support, and thus inhibited the interaction of copper with $Al(OH)_3$ [42]. By correlating the performance and H_2-TPR results, it can be concluded that the strong redox capacity of the $Cu/Al(OH)_3$ catalyst favors the production of alcohols in the plasma-catalytic DRM reaction.

Furthermore, the dependence of the valence state of copper in the $Cu/Al(OH)_3$ catalyst on calcination temperature was investigated using XPS, as shown in Fig. 6(c). While the majority of copper exist in the form of Cu^{2+}, the calcination temperature affects its chemical environment. Specifically, the binding energy of Cu^{2+} shifted towards higher values,

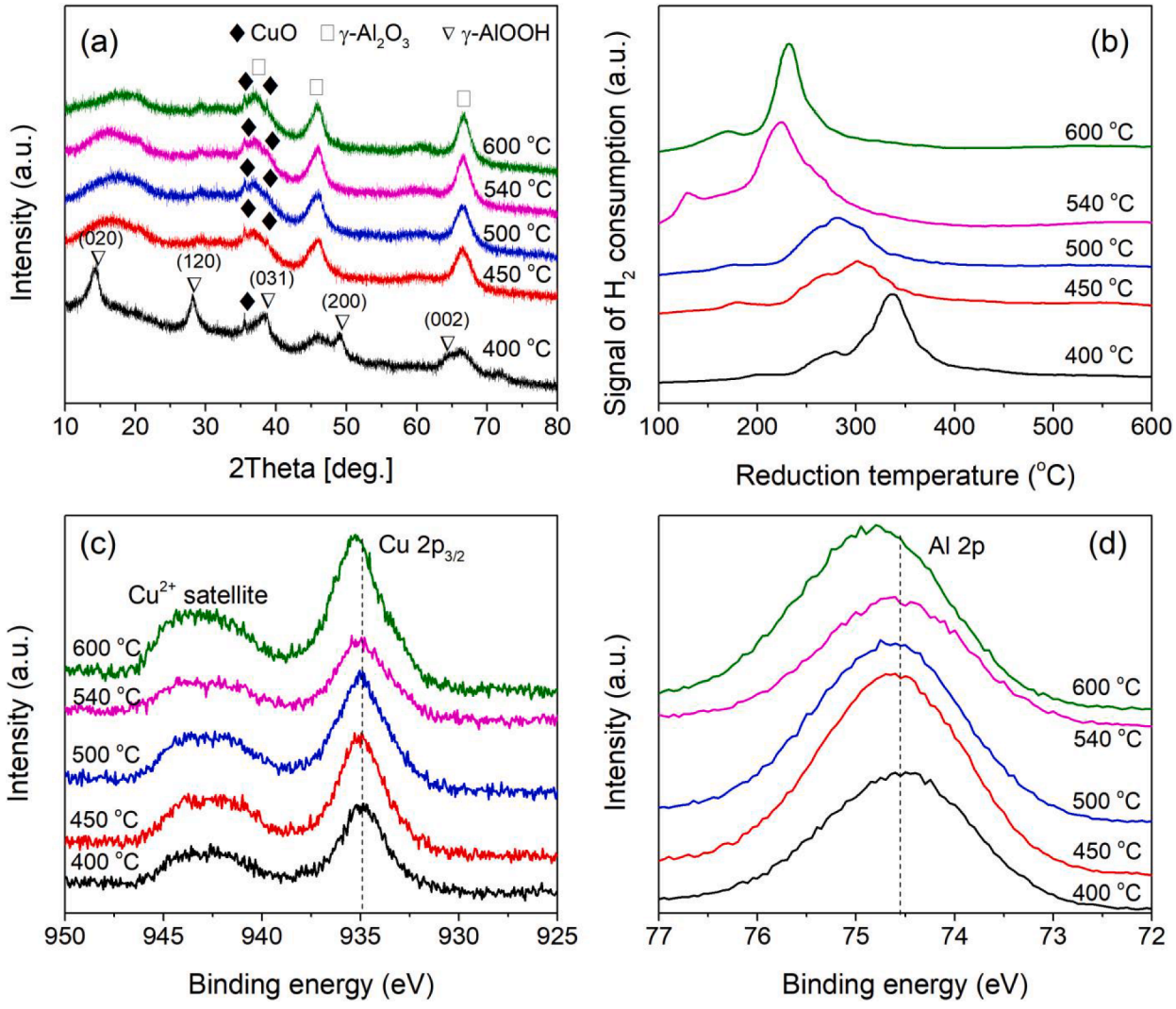

Fig. 6. (a) XRD patterns, (b) H_2-TPR profiles, (c) Cu $2p_{3/2}$ XPS spectra and (d) Al 2p XPS spectra of the $Cu/Al(OH)_3$ catalysts at different calcination temperatures.

especially for samples calcined at high temperatures, such as 540 and 600 °C, compared to those calcined at 400 °C. This shift may be due to the aggregation of monouclear Cu^{2+} species, which was found in Cu/Al_2O_3 catalysts by Bokhoven et al. [52], into nanoparticles at high calcination temperatures. They also revealed monouclear Cu^{2+} species in Cu/Al_2O_3 as the active site for methanol synthesis from methane. In addition, the Al 2p signal located at ~74.5 eV [49] also shifted towards higher binding energy, especially for the sample calcined at 600 °C, as shown in Fig. 6 (d). This shift is mainly attributed to the transformation of Al-OH into Al-O-Al species due to the dehydration of $Al(OH)_3$ at high temperatures, as supported by the XRD results presented in Fig. 6(a).

3.3. Dependence of alcohol generation on copper loading of Cu/Al(OH)$_3$ catalyst.

Using the optimal calcination temperature of 540 °C, we further investigated the catalytic performance of Cu/$Al(OH)_3$ by varying the Cu loading from 1 to 20 wt%. As shown in Fig. 7, the oxygenate selectivity first increased and then decreased with increasing Cu loading, while the opposite trends were observed for both CO and hydrocarbon selectivity. Specifically, the 5 wt%Cu/$Al(OH)_3$ catalyst showed the highest oxygenate selectivity and gas conversion, but the lowest selectivity of gaseous products (i.e., CO and hydrocarbons), as shown in Fig. 7(a)-(d). More importantly, the 5 wt% Cu/$Al(OH)_3$ catalyst maximized the conversion of CH_4 and CO_2 into alcohols with a selectivity of ~38%. Notably, compared to the plasma only system, packing Cu/$Al(OH)_3$ into the plasma area not only enhanced the production of alcohols, but also inhibited the formation of acetic acid. This phenomenon was observed for the Cu/$Al(OH)_3$ catalysts with different Cu loadings, including 1 wt% Cu/$Al(OH)_3$, indicating the critical role of the catalyst in improving alcohol production in the plasma-catalytic DRM reaction.

Interestingly, Fig. 7(b) shows that the ethanol selectivity increased with rising Cu loading, accompanied by a decrease in methanol selectivity. To facilitate visual comparison, we plotted the selectivities of methanol and ethanol as a function of Cu loading (Fig. 8). We found that the optimal Cu loadings for producing methanol and ethanol were 5 wt% and 15 wt%, respectively. As seen from Fig. 8, the Cu/$Al(OH)_3$ catalyst with a Cu loading lower than 10 wt% exhibited a strong capacity for methanol production, while catalysts with a Cu loading of 5–15 wt% greatly promoted ethanol production. To the best of our knowledge, this finding has not been reported up to now, and may provide potential for ethanol production from the plasma-catalytic DRM reaction.

Fig. 9(a) shows the XRD patterns of the Cu/$Al(OH)_3$ catalysts with varying Cu loading. It can be seen that the diffraction peaks of copper species are absent when the Cu loading is below 5 wt%. However, these peaks gradually appear and intensify with increasing Cu loading from 5 to 20 wt%, with the observed diffraction peaks attributed to the characteristic peaks of crystal CuO [31]. The average particle sizes of CuO in

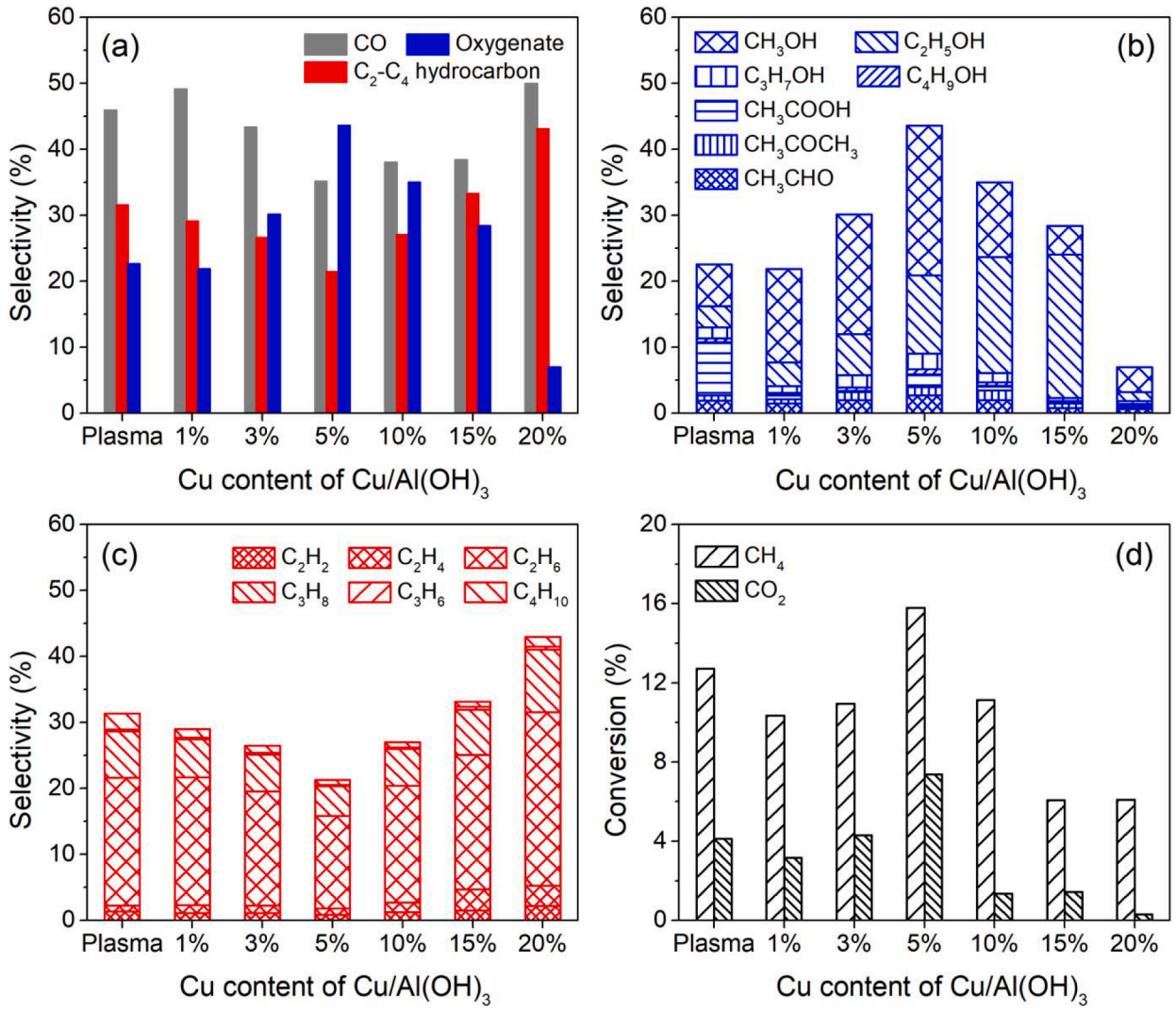

Fig. 7. Dependence of alcohol generation on copper loading of Cu/$Al(OH)_3$ catalyst in plasma-catalytic DRM reaction. (a) Product distribution, (b) Selectivity of oxygenate, (c) Selectivity of gas products and (d) Conversion of CH_4 and CO_2 (reaction temperature was controlled at ~190 °C by tuning discharge power at ~5 W).

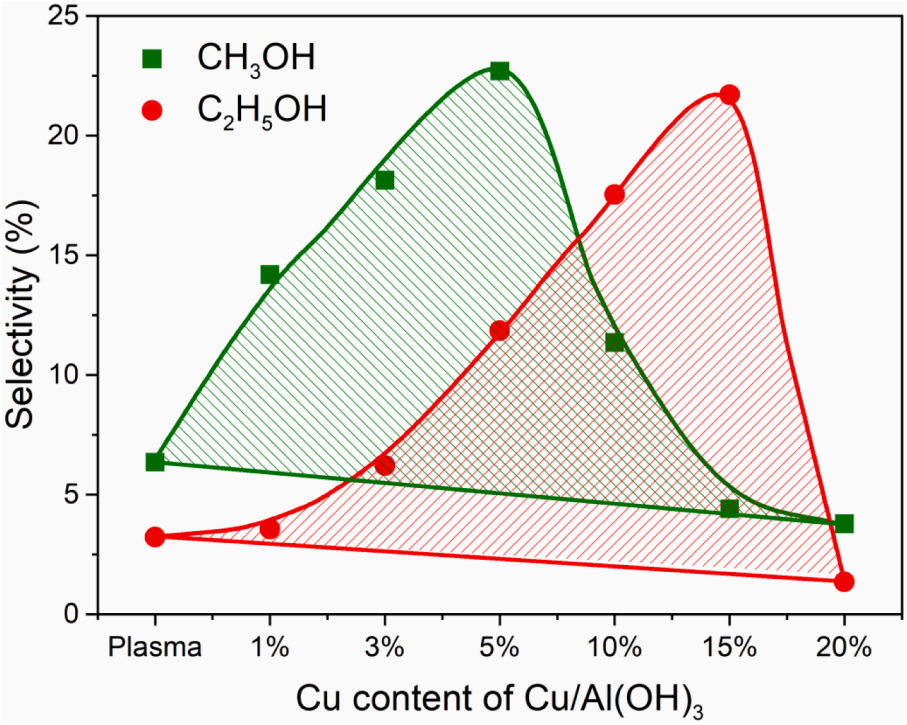

Fig. 8. Selectivities of methanol and ethanol as a function of Cu loading.

the 10, 15 and 20 wt% Cu/Al(OH)$_3$ catalysts were calculated to be approximately 19, 20 and 22 nm, respectively, using Scherrer's formula. Fig. 9(b) presents the influence of Cu loading on the reducible behavior of the Cu/Al(OH)$_3$ catalysts. Clearly, the reduction peak is negligible for the 1 wt% Cu/Al(OH)$_3$ catalyst. However, with the increase in Cu loading from 1 wt% to 5 wt%, the reduction peak becomes visible and gradually shifts to a lower temperature. In contrast, the reduction peak shifts towards a higher temperature and intensifies with Cu loading increasing from 5 wt% to 20 wt%, indicating that large copper particles are predominant in these catalysts, which is supported by the average particle sizes of CuO calculated using Scherrer's formula. As discussed earlier in Fig. 3 (b), the high-temperature reduction peak originates from the one-step reduction of bulk-phase CuO [35–38], while the low-temperature peak is attributed to the reduction of dispersed CuO nanoparticles that strongly bond with the support. In Fig. 9(b), the 5 wt % Cu/Al(OH)$_3$ catalyst exhibits the lowest reduction temperature, indicating the strongest interaction between copper and Al(OH)$_3$, as well as the highest redox capacity of copper species. This is followed by the 10 wt% Cu/Al(OH)$_3$ catalyst, which also exhibits good activity and selectivity for alcohol generation. These findings suggest that the redox capacity of copper species is crucial for alcohol production from the plasma-catalytic DRM reaction.

The reaction rate of oxide-supported metal catalysts is mainly governed by surface reactions, which underscores the significance of active site concentration on the catalyst surface. In this study, increasing the Cu loading markedly boosts the surface copper contents of the Cu/Al(OH)$_3$ catalysts, as demonstrated by the intensified peak intensities of Cu 2p3/2 XPS spectra presented in Fig. 9(c). Moreover, the increased surface copper contains both Cu^{2+} and Cu^{+} species. As mentioned earlier, Cu^{2+} species promote alcohol production, while Cu^{+} species have the opposite effect on the generation of alcohols. Thus, the relationship between alcohol selectivity and Cu^{2+}/Cu^{+} ratio was presented as a function of Cu loading in Fig. 9(d). It can be seen that alcohol selectivity and Cu^{2+}/Cu^{+} ratio exhibit similar trends as the Cu loading increases. The Cu/Al(OH)$_3$ catalysts with higher Cu^{2+}/Cu^{+} ratios demonstrated higher alcohol selectivity, with the most significant difference noted for the catalysts with 5 wt% and 10 wt% Cu loading. However, the 1 wt%- and 20 wt %-Cu/Al(OH)$_3$ catalysts with lower Cu^{2+}/Cu^{+} ratios showed lower alcohol selectivity. These findings effectively account for the decreased alcohol selectivity with Cu loading exceeding 10 wt%, despite the corresponding increase in the total surface content of copper. Therefore, these results demonstrate the beneficial effect of Cu^{2+} species in the Cu/Al(OH)$_3$ catalyst on alcohol generation in the plasma-catalytic DRM reaction.

In addition, tuning the copper loading was the only approach to achieve high ethanol selectivity, while manipulating the support material and calcination temperature did not yield this outcome. Thus, it is hypothesized that the production of ethanol could be related to the particle size of bulk-phase CuO, which needs to be confirmed in future studies through well-designed experiments.

Considering the complex atmosphere (CO_2, CH_4, H_2O and various products) in this study, the state of typical Cu/Al(OH)$_3$ with 5 wt% and 15 wt% Cu loadings was analyzed using XPS before and after the reaction, as shown in Fig. 10. The Cu 2p$_{3/2}$ XPS fitting curves reveal the coexistence of Cu^{2+} and Cu^{+} in these catalysts, but their relative contents changed before and after the reaction. Compared to the fresh catalysts, the Cu^{2+} content of the catalysts decreased, while the Cu^{+} content correspondingly increased after the reaction, as presented in Fig. 10(a). This observation is further supported by the decrease in the Cu^{2+} satellite peak and the Cu LMM Auger spectra in Fig. 10(b). This finding indicates that the catalysts undergo partial reduction in such a complex atmosphere.

4. Conclusion

The plasma-catalytic DRM reaction was investigated for the synthesis of high-value alcohols, including methanol, ethanol, propanol and butanol, using Cu-based catalysts at 190 °C and atmospheric pressure. The selectivity of alcohols was tuned by varying the support material (Al(OH)$_3$, γ-Al_2O_3, TiO_2 and CeO_2), calcination temperature (400, 450, 500, 540 and 600 °C) and copper loading (1–20 wt%) of the Cu-based catalysts. The optimized catalyst was found to be Cu/Al(OH)$_3$, calcined at 540 °C with 5 wt% Cu loading, coupled with DBD plasma, which exhibited the highest alcohol selectivity at around 38%.

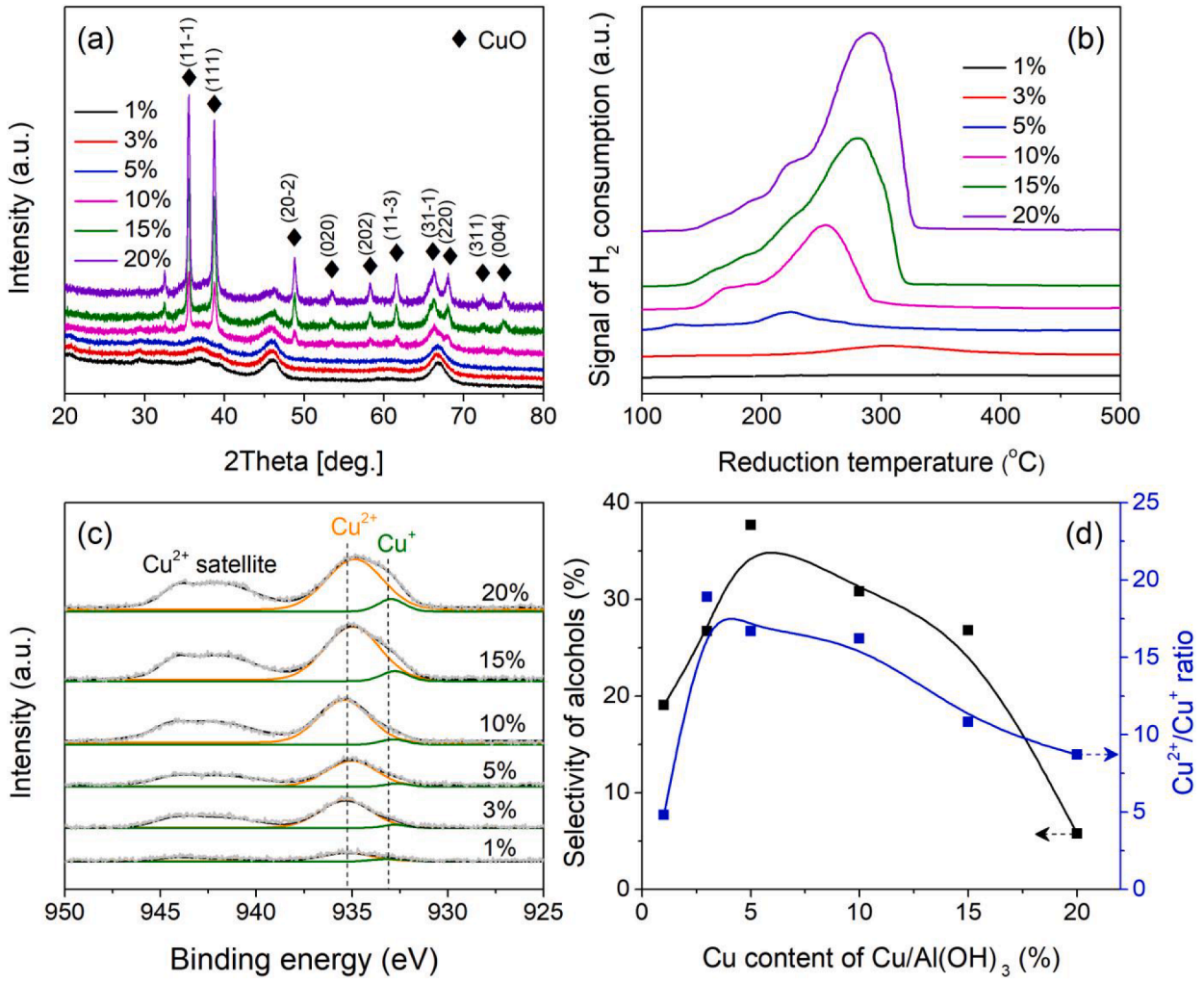

Fig. 9. (a) XRD patterns, (b) H_2-TPR profiles and (c) Deconvoluted Cu $2p_{3/2}$ XPS spectra of the $Cu/Al(OH)_3$ catalysts with different Cu loadings, (d) Selectivity of alcohols and Cu^{2+}/Cu^{+} ratio as a function of Cu content in the $Cu/Al(OH)_3$ catalysts (Cu^{2+}/Cu^{+} ratio was obtained via Fig. 9(c)).

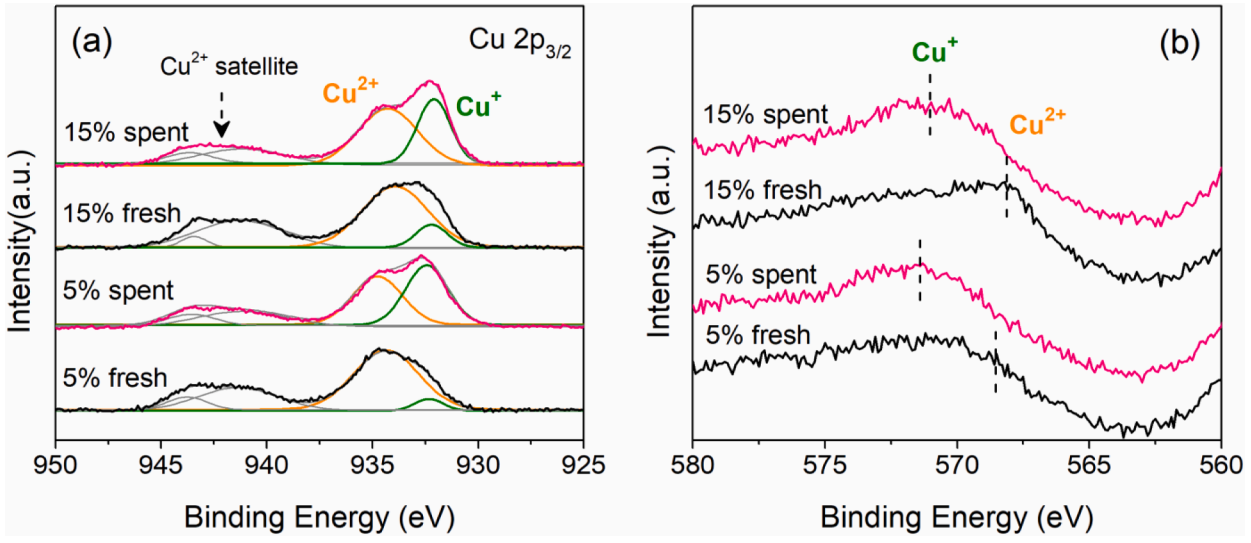

Fig. 10. XPS spectra of $Cu/Al(OH)_3$ catalysts with 5 wt% and 15 wt% Cu loadings before and after the reaction. (a) Deconvoluted Cu $2p_{3/2}$ XPS spectra, (b) Cu LMM Auger spectra.

Furthermore, the characterization of the catalysts revealed that the redox capacity and valence state of copper species are crucial for alcohol formation during the plasma-catalytic DRM reaction. The support material, calcination temperature and copper loading can be used to manipulate these two properties of the catalysts. Specifically, the catalysts with a strong redox capacity and abundant Cu^{2+} species were found to promote alcohol production.

Interestingly, methanol is commonly reported as the major product in the produced alcohols. However, at high Cu loading, the predominant alcohol in the products shifts from methanol to ethanol, with the optimal copper loadings for producing methanol and ethanol being 5 wt% and 15 wt%, respectively. This finding opens the door to the direct synthesis of ethanol from the plasma-catalyzed DRM reaction under mild conditions. However, further studies are necessary to better understand this process and its underlying reaction mechanisms. This work demonstrates the feasibility of using Cu-based catalysts for the plasma-catalytic conversion of CH_4 and CO_2 into high-value alcohols and highlights the importance of optimizing catalyst composition and reaction conditions to achieve high selectivity and yield of alcohols under ambient conditions. Future research should focus on the rational design of catalysts to enhance the selectivity of alcohols and the stability of the catalysts for the plasma-catalytic conversion of CH_4 and CO_2 into high-value alcohols.

Declaration of Competing Interest

The authors declare that they have no known competing financial interests or personal relationships that could have appeared to influence the work reported in this paper.

Data availability

Data will be made available on request.

Acknowledgements

We acknowledge the financial support from the National Natural Science Foundation of China (21908016), PetroChina Innovation Foundation (2019D-5007-0407) and the LiaoNing Revitalization Talents Program (XLYC1907008). X. Tu acknowledges the funding from the European Union's Horizon 2020 research and innovation programme under the Marie Sklodowska-Curie grant agreement No. 823745.

References

[1] V. Turan, P. Schröder, S. Bilen, H. Insam, M.F.D. Juárez, Co-inoculation efect of Rhizobium and Achillea millefolium L. oil extracts on growth of common bean (Phaseolus vulgaris L.) and soil microbial-chemical properties, Sci. Rep. 9 (2019) 15178–15187.
[2] V. Turan, Confident performance of chitosan and pistachio shell biochar on reducing Ni bioavailability in soil and plant plus improved the soil enzymatic activities, antioxidant defense system and nutritional quality of lettuce, Ecotoxicol. Environ. Saf. 183 (2019) 109594.
[3] V. Turan, Potential of pistachio shell biochar and dicalcium phosphate combination to reduce Pb speciation in spinach, improved soil enzymatic activities, plant nutritional quality, and antioxidant defense system, Chemosphere. 245 (2020) 125611.
[4] V. Turan, Arbuscular mycorrhizal fungi and pistachio husk biochar combination reduces Ni distribution in mungbean plant and improves plant antioxidants and soil enzymes, Physiol. Plantarum. 173 (2021) 418–429.
[5] V. Turan, Calcite in combination with olive pulp biochar reduces Ni mobility in soil and its distribution in chili plant, Int. J. Phytoremediat. 24 (2022) 166–176.
[6] A. Bogaerts, X. Tu, J.C. Whitehead, G. Centi, L. Lefferts, O. Guaitella, F. Azzolina-Jury, H.-H. Kim, A.B. Murphy, W.F. Schneider, T. Nozaki, J.C. Hicks, A. Rousseau, F. Thevenet, A. Khacef, M. Carreon, plasma catalysis roadmap, J. Phys. D: Appl. Phys. 53 (2020) 443001.
[7] A. George, B. Shen, M. Craven, Y. Wang, D. Kang, C. Wu, X. Tu, A review of non-thermal plasma technology: a novel solution for CO_2 conversion and utilization, Renew. Sust. Energ. Rev. 135 (2021) 109702.
[8] S. Liu, L.R. Winter, J.G. Chen, Review of plasma-assisted catalysis for selective generation of oxygenates from CO_2 and CH_4, ACS Catal. 10 (2020) 2855–2871.
[9] H. Puliyalil, D. Lašič Jurković, V.D.B.C. Dasireddy, B. Likozar, A review of plasma-assisted catalytic conversion of gaseous carbon dioxide and methane into value-added platform chemicals and fuels, RSC Adv. 8 (2018) 27481–27508.
[10] Y. Wang, Y. Chen, J. Harding, H. He, A. Bogaerts, X. Tu, Catalyst-free single-step plasma reforming of CH_4 and CO_2 to higher value oxygenates under ambient conditions, Chem. Eng. J. 450 (2022) 137860.
[11] L. Yang, C. Liu, E. Baldur, Y. Wang, Synthesis of oxygenates and higher hydrocarbons directly from methane and carbon dioxide using dielectric-barrier discharges: product distribution, Energ, Fuel. 16 (2002) 864–870.
[12] G. Scarduelli, G. Guella, D. Ascenzi, P. Tosi, Synthesis of liquid organic compounds from CH_4 and CO_2 in a dielectric barrier discharge operating at atmospheric pressure, Plasma Process. Polym. 8 (2011) 25–31.
[13] L.M. Martini, G. Dilecce, G. Guella, A. Maranzana, G. Tonachini, P. Tosi, Oxidation of CH_4 by CO_2 in a dielectric barrier discharge, Chem. Phys. Lett. 593 (2014) 55–60.
[14] T. Kolb, J.H. Voigt, K.-H. Gericke, Conversion of methane and carbon dioxide in a DBD reactor: influence of oxygen, Plasma Chem. Plasma Process. 33 (2013) 631–646.
[15] K. Krawczyk, M. Młotek, B. Ulejczyk, K.S. Szałowski, Methane conversion with carbon dioxide in plasma-catalytic system, Fuel. 117 (2014) 608–617.
[16] A. Rahmani, M. Nikravech, Impact of argon in reforming of (CH_4+ CO_2) in surface dielectric barrier discharge reactor to produce syngas and liquid fuels, Plasma Chem. Plasma Process. 38 (2018) 517–534.
[17] I. Michielsen, Y. Uytdenhouwen, A. Bogaerts, V. Meynen, Altering conversion and product selectivity of dry reforming of methane in a dielectric barrier discharge by changing the dielectric packing material, Catal. 9 (2019) 51–82.
[18] J.F. Gelves, L. Dorkis, M. Marquez, E. Fourré, C.B. Dupeyrat, Synthesis of oxygenated compounds from methane, carbon dioxide and water in liquid phase using a plasma-catalytic system, J. Phys. Conf. Ser. 1386 (2019), 012045.
[19] D.i. Li, V. Rohani, F. Fabry, A. Parakkulam Ramaswamy, M. Sennour, L. Fulcheri, Direct conversion of CO_2 and CH_4 into liquid chemicals by plasma-catalysis, Appl. Catal. B: Environ. 261 (2020) 118228.
[20] J. Li, L. Dou, Y. Gao, X. Hei, F. Yu, T. Shao, Revealing the active sites of the structured Ni-based catalysts for one-step CO_2/CH_4 conversion into oxygenates by plasma-catalysis, J. CO_2 Util. 52 (2021) 101675.
[21] L. Dou, Y. Liu, Y. Gao, J. Li, X. Hu, S. Zhang, K. Ostrikov, T. Shao, Disentangling metallic cobalt sites and oxygen vacancy effects in synergistic plasma-catalytic CO_2/CH_4 conversion into oxygenates, Appl. Catal. B: Environ. 318 (2022) 121830.
[22] A. Wang, J.H. Harrhy, S. Meng, P. He, L. Liu, H. Song, Nonthermal plasma-catalytic conversion of biogas to liquid chemicals with low coke formation, Energy Conv. Manag. 191 (2019) 93–101.
[23] A.N. Biswas, L.R. Winter, B. Loenders, Z. Xie, A. Bogaerts, J.G. Chen, Oxygenate production from plasma-activated reaction of CO_2 and ethane, ACS Energy Lett. 7 (2022) 236–241.
[24] M. Shirazi, E.C. Neyts, A. Bogaerts, DFT study of Ni-catalyzed plasma dry reforming of methane, Appl. Catal. B: Environ. 205 (2017) 605–614.
[25] D. Mei, M. Sun, S. Liu, P. Zhang, Z. Fang, X. Tu, Plasma-enabled catalytic dry reforming of CH_4 into syngas, hydrocarbons and oxygenates: Insight into the active metals of γ-Al_2O_3 supported catalysts, J. CO_2 Util. 67 (2023) 102307.
[26] Y. Li, H. Yu, J. Dai, Z. Zhang, Z. Zhang, H. Yu, L. Liu, CH_4 and CO_2 conversion over boron nitride-supported Ni catalysts with B-O defects in DBD plasma, Fuel Process. Technol. 242 (2023) 107655.
[27] L.i. Wang, Y. Yi, C. Wu, H. Guo, X. Tu, One-step reforming of CO_2 and CH_4 into high-value liquid chemicals and fuels at room temperature by plasma-driven catalysis, Angew. Chem. Int. Edit. 56 (2017) 13679–13683.
[28] Y. Wang, L. Fan, H. Xu, X. Du, H. Xiao, J.i. Qian, Y. Zhu, X. Tu, L.i. Wang, Insight into the synthesis of alcohols and acids in plasma-driven conversion of CO_2 and CH_4 over copper-based catalysts, Appl. Catal. B: Environ. 315 (2022) 121583.
[29] Y. Yi, C. Xu, L. Wang, J. Yu, Q. Zhu, S. Sun, X. Tu, C. Meng, J. Zhang, H. Guo, Selectivity control of H_2/O_2 plasma reaction for direct synthesis of high purity H_2O_2 with desired concentration, Chem. Eng. J. 313 (2017) 37–46.
[30] B. Huang, C. Zhang, H. Bai, S. Zhang, K. Ostrikov, T. Shao, Energy pooling mechanism for catalyst-free methane activation in nanosecond pulsed non-thermal plasmas, Chem. Eng. J. 396 (2020) 125185.
[31] F.C.F. Marcos, R.S. Alvim, L. Lin, L.E. Betancourt, D.D. Petrolini, S.D. Senanayake, R.M.B. Alves, J.M. Assaf, J.A. Rodriguez, R. Giudici, E.M. Assaf, The role of copper crystallization and segregation toward enhanced methanol synthesis via CO_2 hydrogenation over $CuZrO_2$ catalysts: A combined experimental and computational study, Chem. Eng. J. 452 (2023) 139519.
[32] J. Yu, Q. Guo, X. Xiao, H. Mao, D. Mao, J. Yu, High-heat treatment enhanced catalytic activity of CuO/CeO_2 catalysts with low CuO content for CO oxidation, Catal, Sci. Technol. 10 (2020) 5256–5266.
[33] Y. Liu, D. Mao, J. Yu, Y. Zheng, X. Guo, Facile preparation of highly active and stable CuO-CeO_2 catalysts for low-temperature CO oxidation via a direct solvothermal method, Catal, Sci. Technol. 10 (2020) 8383–8395.
[34] Z. Guerra-Que, H. Pérez-Vidal, G. Torres-Torres, J.C. Arévalo-Pérez, A.A.S. Pavón, A. Cervantes-Uribe, A.E.D.L. Monteros, M.A. Lunagómez-Rocha, Treatment of phenol by catalytic wet air oxidation: a comparative study of copper and nickel supported on γ-alumina, ceria and γ-alumina-ceria, RSC Adv. 9 (2019) 8463–8479.
[35] Y. He, Z.S. Fishman, K.R. Yang, B. Ortiz, C. Liu, J. Goldsamt, V.S. Batista, L. D. Pfefferle, Hydrophobic CuO nanosheets functionalized with organic adsorbates, J. Am. Chem. Soc. 140 (2018) 1824–1833.
[36] M. Liao, C. Guo, W. Guo, T. Hu, J. Xie, P. Gao, H. Xiao, One-step growth of $CuO/ZnO/CeO_2/ZrO_2$ nanoflowers catalyst by hydrothermal method on Al_2O_3 support for methanol steam reforming in a microreactor, Int. J. Hydrogen Energ. 46 (2021) 9280–9291.

[37] S. Yang, F. Zhou, Y. Liu, L. Zhang, Y.u. Chen, H. Wang, Y. Tian, C. Zhang, D. Liu, Morphology effect of ceria on the performance of CuO/CeO_2 catalysts for hydrogen production by methanol steam reforming, Int. J. Hydrogen Energ. 44 (2019) 7252–7261.
[38] K. Nakagawa, T. Ohshima, Y. Tezuka, M. Katayama, M. Katoh, S. Sugiyama, Morphological effects of CeO_2 nanostructures for catalytic soot combustion of CuO/CeO_2, Catal. Today. 246 (2015) 67–71.
[39] I.U. Dina, M.S. Shaharunb, A. Naeemc, S. Tasleemd, M.R. Johan, Carbon nanofibers based copper/zirconia catalysts for carbon dioxide hydrogenation to methanol: Effect of copper concentration, Chem. Eng. J. 334 (2018) 619–629.
[40] Y. Gao, Z. Zhang, Z. Li, W. Huang, Understanding morphology-dependent CuO_x-CeO_2 interactions from the very beginning, Chinese, J. Catal. 41 (2020) 1006–1016.
[41] S.J. Tauster, S.C. Fung, R.L. Garten, Strong metal-support interactions. Group 8 noble metals supported on TiO_2, J. Am. Chem. Soc. 9 (1978) 170–175.
[42] Q. Fu, T. Wagner, Interaction of nanostructured metal overlayers with oxide surfaces, Surf. Sci. Rep. 62 (2007) 431–498.
[43] P. Hu, Z. Huang, Z. Amghouz, M. Makkee, F. Xu, F. Kapteijn, A. Dikhtiarenko, Y. Chen, X. Gu, X. Tang, Electronic metal-support interactions in single-atom catalysts, Angew. Chem. Int. Ed. 53 (2014) 3418–3421.
[44] H. Tang, F. Liu, J. Wei, B. Qiao, K. Zhao, Y. Su, C. Jin, L. Li, J.(. Liu, J. Wang, T. Zhang, Ultrastable hydroxyapatite/titanium-dioxide-supported gold nanocatalyst with strong metal-support interaction for carbon monoxide oxidation, Angew. Chem. Int. Ed. 55 (2016) 10606–10611.
[45] J.P. Espinós, J. Morales, A. Barranco, A. Caballero, J.P. Holgado, A.R. González-Elipe, Interface effects for Cu, CuO, and Cu_2O deposited on SiO_2 and ZrO_2. XPS determination of the valence state of Copper in Cu/SiO_2 and Cu/ZrO_2 catalysts, J. Phys. Chem. 106 (2002) 6921–6929.
[46] T. Ghodselahi, M.A. Vesaghi, A. Shafiekhani, A. Baghizadeh, M. Lameii, XPS study of the $Cu@Cu_2O$ core-shell nanoparticles, Appl. Surf. Sci. 255 (2008) 2730–2734.
[47] Y. An, M. Han, H. Zheng, W. Ding, Q. Sun, C. Hu, L. Zheng, Hollow structured copper-loaded self-floating catalyst in sulfite-induced oxidation of arsenic(III) at neutral pH: Kinetics and mechanisms investigation, Chem. Eng. J. 407 (2021) 127193.
[48] A. Chen, X. Yu, Y. Zhou, S. Miao, Y. Li, S. Kuld, J. Sehested, J. Liu, T. Aoki, S. Hong, M.F. Camellone, S. Fabris, J. Ning, C. Jin, C. Yang, A. Nefedov, C. Wöll, Y. Wang, W. Shen, Structure of the catalytically active copper-ceria interfacial perimeter, Nat. Catal. 2 (2019) 334–341.
[49] P. Li, S. Zheng, P. Qing, Y. Chen, L. Tian, X. Zheng, Y.i. Zhang, The vanadate adsorption on a mesoporous boehmite and its cleaner production application of chromate, Green Chem. 16 (2014) 4214–4222.
[50] H. Zhang, P. Li, Z. Wang, X. Zhang, S. Zheng, Y. Zhang, In situ synthesis of γ-AlOOH and synchronous adsorption separation of V(V) from highly concentrated Cr(VI) multiplex complex solutions, ACS Sustain. Chem. Eng. 5 (2017) 6674–6681.
[51] Y. Liu, S. Qing, X. Hou, F. Qin, X. Wang, Z. Gao, H. Xiang, Temperature dependence of Cu-Al spinel formation and its catalytic performance in methanol steam reforming, Catal Sci. Technol. 7 (2017) 5069–5078.
[52] J. Meyet, A. Ashuiev, G. Noh, M.A. Newton, D. Klose, K. Searles, A.P.V. Bavel, A. D. Horton, G. Jeschke, J.A.V. Bokhoven, C. Coperet, Methane-to-methanol on mononuclear copper(II) sites supported on Al_2O_3: structure of active sites from electron paramagnetic resonance, Angew. Chem. 133 (2021) 16336–16343.